Simulation of Microstructure/Mechanism Relationships in Particle Deposition

The important connection between particulate deposit properties and deposition mechanism remains poorly understood and only scarcely studied. Accordingly, in this research, we develop a discrete stochastic model to simulate particulate deposition processes resulting from realistic combinations of deposition mechanisms. Particle motion is assumed to be determined by the superposition of a deterministic force that acts toward the collecting surface and a random force, which produces Brownian diffusion. We characterize the resulting deposit microstructure via porosity and pore size/area distribution, surface area; and we examine the evolution of these descriptors with time (number of particles deposited) for different deposition mechanisms. We also examine the effect of particle polydispersity, spatial orientation (for nonspherical particles), and mean-free-path on the resulting deposit structure.

M. Tassopoulos
J. A. O'Brien
D. E. Rosner
Yale University
Department of Chemical Engineering
HTCRE Laboratory
New Haven, CT 06520

Introduction

The deposition on exposed surfaces of particles (and, often simultaneously, condensable vapors) is of importance in many technologies. Often, deposition is undesirable (leading to corrosion and fouling, as in combustion turbines and heat exchangers) while, in other cases, commercial processes rely on carefully controlled particle and/or vapor deposition (e.g., fabrication of optical wave-guides and coatings). In all cases the transport properties of the resulting deposit (thermal conductivity, permeability, etc.), which, of course, depend on the deposit microstructure, are factors that determine the technological and economic feasibility of the process.

Predictions of deposit growth rate and associated microstructure are often difficult to make since they involve large-scale movements of the particle-laden host fluid and small-scale interactions (at the particle level). In the general formulation of such problems, it is useful to distinguish three different types of interactions:

1. Host fluid-suspended particle interactions
2. Particle-particle interactions while the particles are dispersed (usually negligible, even in highly mass loaded aerosol systems; see, Rosner and Park, 1988)
3. Depositing particle-deposit interactions modeled below

Calculations of particle deposition rates, under many commonly encountered ambient conditions, and for different driving mechanisms have been carried out by various authors *without* focusing on the microstructure of the resulting deposits. Thus, illustrative solutions have been obtained, either using analytical-numerical techniques (see, e.g., Fuchs, 1964; Friedlander, 1977; Goren, 1977; Gökoglu and Rosner, 1986; Park and Rosner, 1989; Rosner, 1989) or from stochastic simulations of representative particle trajectories (Tien et al., 1977; Gupta and Peters, 1984).

Interactions between depositing particles and small numbers of previously deposited particles have been also studied, primarily from a filtration viewpoint. For example, various models have been proposed to determine the dependence of filter (fiber) capture efficiency on particle accumulation (Tien, 1982; Davies, 1966). However, because these models are intended to predict the evolution of filter performance, they often ignore the microstructure of the deposits (e.g., filter cake) grown by the captured particles. In most of these applications, it has been sufficient to simply keep track of the wetted area of the deposit, presumed to determine secondary collection, and perhaps the net charge of the fibers in the case of electrostatic fibers. In contrast, we are concerned here with applications in which the deposit microstructure and associated deposit transport properties are especially important to the performance of the system.

We expect that for any deposition process there is a dynamic coupling between the deposition mechanism and the deposit microstructure. Thus, a sufficiently complete description of the deposition process should not only provide information about the driving mechanism and associated particle deposition *rates*, but also about the resulting deposit *microstructure*. Stochastic particle trajectory methods (Tien et al., 1977; Peters et al., 1985) can be extended in a straightforward way to generate the deposit

microstructure on a particle-by-particle basis as the deposition proceeds. However, the main disadvantage of such methods is that the requirements in both computer memory and computer time increase in a highly nonlinear way with the size of the system, so one is practically confined to excessively small size systems (~500 particles).

To overcome these limitations, we present here a realistic and versatile, yet tractable, model in two- and three-dimensions, in which we computer-generate deposits on orthogonal lattices with every particle following an *asymmetric* random walk trajectory in the vicinity of the deposit. In fact, this model is a generalization of two recently investigated stochastic growth models, namely the ballistic aggregation and diffusion limited aggregation (DLA) models. Required properties of the resulting deposit, e.g., surface area, internal temperature distribution, or any other relevant quantity, can be computed and updated as the deposition proceeds (addition of new particles), so that the required relationships between the deposition mechanism and the resulting deposit microstructure can be established. Note that, at this stage, we assume the deposition mechanisms to be invariant throughout the deposition process. Future work will relax the latter assumption.

Simpler, two-dimensional versions of biased diffusion models have been described elsewhere (Kapral et al., 1986; Houi and Lenormand, 1984). The present work is more general since:

1) We do not limit ourselves to two dimensions and, further, we consider the effects of polydisperse particle populations, spatial orientation in the case of elongated particles, and particle "mean-free-path," on the resulting microstructure. Clearly these factors are relevant from a practical viewpoint and, furthermore, give rise to interesting results.

2) We establish a closer connection between a 'real-life' deposition problem and the corresponding on-lattice computer simulations.

3) The existing literature on the model (see, e.g., Houi and Lenormand, 1984) is not very accessible to engineers.

(In fact, we formulated the model independently, and only later discovered the previous work. Furthermore, we define the dimensionless parameter used to interpret our data in a different way, which turns out to be more general, as will be discussed in the following section.)

First, we will describe the stochastic model and demonstrate how it accounts for the deposit microstructures associated with different combinations of commonly encountered deposition mechanisms. We will also outline our algorithm and results, as well as the implications of these interrelationships.

Stochastic Model of Particulate Deposition

In recent years, extensive research has been conducted on so-called "stochastic growth" or "aggregation models" (for a review, see Stanley and Ostrowsky, 1986; Family and Landau, 1984). Such models are of interest, because they can be related to observed physical phenomena and because, despite their simplicity, they sometimes give rise to scale-invariant or 'fractal' structures (Mandelbrot, 1983). Our approach is a tractable extension of these models, applied here to two- and three-dimensional idealizations of *line* or *surface* deposits.

Figure 1 shows a schematic representation of a particulate deposit grown on a two-dimensional orthogonal lattice. We assume here that the particles arrive one at a time and that each particle trajectory can be represented by a biased random walk. In Figure 1, p_1 is the probability that the particle will move south in the next step, p_2 east, etc., so that

$$\sum_{i=1}^{2d} p_i = 1 \tag{1}$$

where d is the dimensionality of the lattice (here $d = 2$ or 3).

If all transition probabilities are equal, e.g., $p_1 = p_2 = \cdots = p_{2d} = 1/(2d)$, we obtain the *diffusion-limited aggregation model* (Witten and Sander, 1981). The DLA model simulates the growth of an aggregate under isotropic diffusion-limited conditions, i.e., the depositing particles undergo equilibrium Brownian motion.

If, on the other hand, we set the probability of moving toward the deposit, p_1, equal to unity, we obtain the so-called *ballistic aggregation model* (Vold, 1963; Meakin et al., 1986). According to the ballistic model, every particle follows a straight line trajectory, so that this model can simulate growth due to sedimentation, impaction, or some predominantly 'phoretic' mechanism such as thermophoresis, photophoresis, or electrophoresis.

In practical deposition processes, many of the above-mentioned mechanisms for growth, namely, Brownian diffusion, impaction and phoresis, can occur *simultaneously* (see e.g., Fernandez de la Mora and Rosner 1981; Park and Rosner, 1989; Castillo et al., 1989; Houi and Lenormand, 1984). Hence, a generally useful model should be able to account for combinations of these mechanisms. With these considerations in mind, if we denote by $x(t)$ the position of a particle at time t, then it can be represented by

$$x(t) = \tilde{x}(t) + \int_0^t c\, dt \tag{2}$$

where $\tilde{x}(t)$ is a Brownian process, and $c(x, t)$ is the local deterministic velocity, not necessarily independent of position and/or time. (In our context, time is an appropriate function of the number of particles already deposited.) Equation 2 may be viewed as the trajectory predicted from the Langevin equation (Albers et al., 1970). Note from Eq. 2 that in the absence of the drift velocity, c, each particle would follow a pure Brownian or *random walk* motion. Next we discretize both the space and the target, and set the unit cell size equal to the characteristic length of a particle. The description of this motion using a length scale equal to the particle size is expected to be accurate for Stokesian or transition regime particles where the particle 'jump distance' is of the same order as or less than the particle size. Note, however, that for Knudsen aerosols (or heavy molecules, for that matter; see, e.g., Garcia-Ybarra and Rosner, 1988), each step can be significantly larger than the particle size and, hence, a new length scale, the particle mean-free-path (jump distance), enters the problem. The effect of this new length scale will be discussed later. In a discrete frame of reference, the particle trajectory becomes a random walk with asymmetric jumps in the general case. Clearly, a random walk cannot duplicate exactly a continuous motion; rather, by correctly assigning the transition probabilities at each step, it simulates the continuous motion on the average at the length scale of the unit cell.

In this introductory paper, we focus on deposit growth where the particle motion is caused by a constant force directed toward a target surface *in the simultaneous presence of Brownian diffusion.* In this case, we introduce κ as a transition parameter, varying between 0 and 1, being equal to unity in the limiting

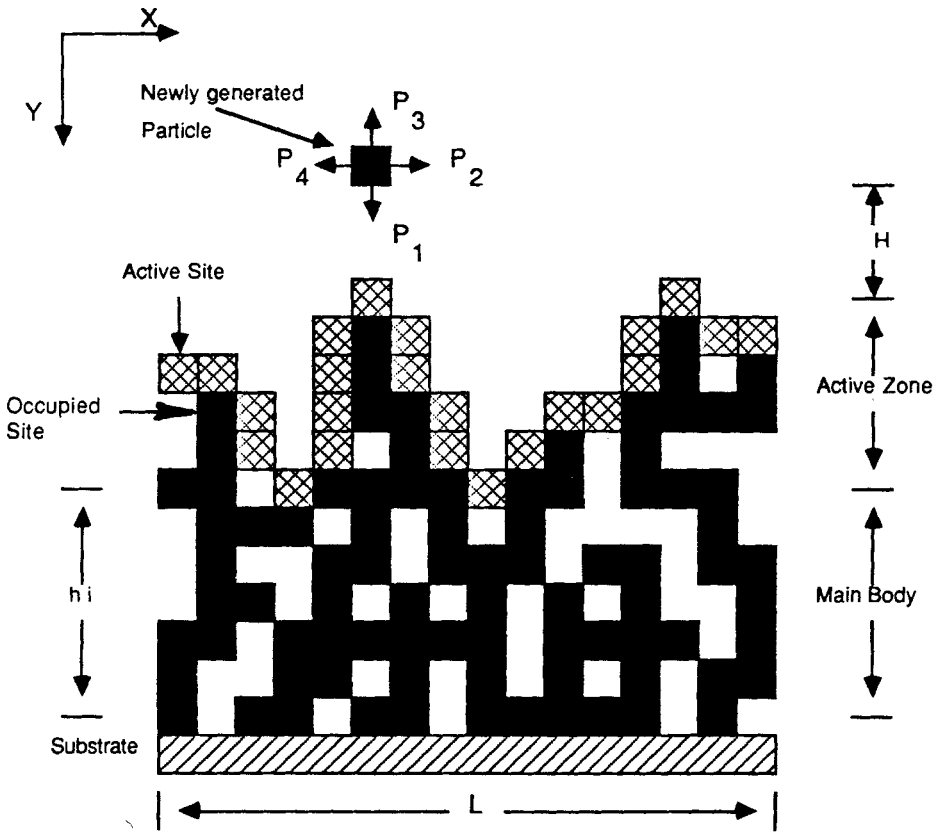

Figure 1. Particulate deposit computer-grown on a two-dimensional orthogonal lattice.
Black squares represent occupied sites and crossed squares represent the currently active sites. H is the distance from the top of the deposit where each new particle is generated.

case of pure diffusion and equal to zero for pure ballistic motion toward the collecting target. The probability of diffusing in any direction is then the same and equal to $\kappa/(2d)$, and the probability of moving towards the target in the next step, is given by

$$p_1 = (1 - \kappa) + \frac{\kappa}{(2d)} \tag{3}$$

so that the sum of the probabilities is always equal to unity.

In problems where the motion is due to a stochastic part such as diffusion and a deterministic part such as convection, phoresis, etc., the relative importance of the two mechanisms may also be expressed in terms of a dimensionless Peclet number (see, e.g., Rosner, 1986). The latter, which we relate to κ below, can be viewed as the ratio of a characteristic time for diffusion to a characteristic time for convection, e.g.

$$Pe = \frac{t_{\text{diffusion}}}{t_{\text{convection}}} = \left(\frac{\delta_m^2}{D_B}\right) \Big/ \left(\frac{\delta_m}{V}\right) \tag{4}$$

Here, V is the velocity due to the deterministic motion (in the original definition of the Peclet number, it would be the convective velocity), δ_m is some relevant characteristic length and D_B is the Brownian diffusion coefficient.

The deterministic velocity, V, towards the target is given by the distance traveled in a certain time (say $n\tau$, τ being the time step and n being the number of steps). In n steps, the expected distance traveled, which is clearly due to the deterministic force, is $(1 - \kappa) \cdot n \cdot l$, and so

$$V = \frac{(1 - \kappa)nl}{n\tau} = \frac{(1 - \kappa)l}{\tau} \tag{5}$$

where l is the particle mean-free-path, e.g., the distance traveled by the particle before there is a significant change of its velocity. Note that since we consider only on-lattice simulations, l must always be an integer multiple of the particle (lattice) size.

The diffusion coefficient for a d-dimensional asymmetric random walk (for the exact derivation see Appendix A) can be defined by:

$$D_B = \frac{\overline{(x - \bar{x})^2}}{2dt} = \frac{\kappa(2 - \kappa)l^2}{2d\tau} \tag{6}$$

Substituting Eqs. 5 and 6 into Eq. 4, we obtain the equivalent of the Peclet number for a d-dimensional orthogonal lattice

$$Pe = \frac{2d(1 - \kappa)}{\kappa(2 - \kappa)} \frac{\delta_m}{l} \tag{7}$$

Initially we will take the characteristic length δ_m to be equal to the particle size, a, i.e.

$$\delta_m = a \tag{8}$$

and further assume that the particle mean free path is also equal to the particle size, e.g.

$$l = a \tag{9}$$

Under these assumptions, Eq. 7 yields,

$$Pe = \frac{2d(1-\kappa)}{\kappa(2-\kappa)} \tag{10}$$

Note that for the limiting case of no diffusion ($\kappa = 0$, pure ballistic case) this Peclet number goes to infinity, and for the limiting case of no drift ($\kappa = 1$, pure DLA) Pe tends to zero. The Peclet number as defined here is different from the Peclet number of Houi and Lenormand (Eq. 3, 1984), due to the appearance of the $(2 - \kappa)$ factor in our definition. In fact, the Peclet number as defined by Houi and Lenormand, is exact only for the case of pure diffusion. In the latter regime, the switching parameter κ, is close to unity, and the two definitions become equivalent.

The Algorithm

At this stage, we carry out our deposition simulations on two- and three-dimensional square and cubic lattices, respectively, with periodic boundary conditions. (Periodic boundary conditions are introduced in order to avoid edge effects arising from the finite width of the lattice.) We decided to carry out our initial simulations under these simplifying assumptions (i.e., two- and three-dimensional "on-lattice" as opposed to three-dimensional "off-lattice") because

a) There is already evidence in the literature that in both cases the *qualitative* behavior is the same (compare, e.g., Meakin et al., 1986; Baumgartner and Löffler, 1987; Houi and Lenormand, 1984).

b) A sufficiently detailed description of the resulting microstructure would be prohibitively time-consuming for deposits grown off-lattice.

c) We wanted to evaluate our general approach using the simplest model capable of accounting for the essential features of a real deposition process.

Each particle is introduced at a randomly selected position at a height $h_{max} + H$ (Figure 1) above the target, where h_{max} is the maximum height measured in particle diameters for the center of any particle in the deposit, and H is an assigned distance, perhaps equal to the thickness of an equivalent mass diffusion Brownian sublayer (Gokoglu and Rosner, 1986). Note that the boundary layer approximation that we implicitly make, when we introduce the starting distance H, will be valid only if

$$H \sim Re^{-1/2}Sc^{-1} \gg \xi \tag{11}$$

where Re is the target based Reynolds number, Sc the Schmidt number, and ξ, a measure of the deposit surface roughness, will be defined later. We describe as *active* sites the *empty* sites on the free surface of the deposit that can be occupied by the next particle (see caption of Figure 1). In our simulations, we define them using a nearest-neighbor (NN) model. According to the NN model, active sites are those which are nearest neighbors of the occupied sites of the deposit-free surface.

We define as the *main body* the lower part of the deposit that is not affected by subsequent particle arrivals. The interfacial region, the upper part of the deposit in Figure 1, we term the *active zone* (see also Meakin et al., 1986). Note that, while for the pure ballistic case it corresponds only to one active site per lattice column (e.g., definition of Meakin, 1986), in the case of ballistic deposition in the simultaneous presence of diffusion, it is possible to have more than one active site per column (see Figure 1).

Each iteration proceeds as follows. We generate a particle at a distance H over the growing interface and allow it to perform a biased random walk governed by the transition probabilities p_1, $p_2, \ldots, p_{2d}$, until it either arrives at an active site, at which it is assumed to stick irreversibly, or it wanders too far away from the deposit, so that we remove it. In the present simulations, we remove a particle if it reaches a distance from the collecting target more than three times the current maximum height of the deposit. We repeat this biased random walk procedure once for each particle we wish to deposit.

If we further denote by $h_i(h_{ij})$, the height of the deposit at site $i(ij)$ for two- (or three-) dimensions, then the mean height of the deposit, $\bar{h}$, can be defined by

$$\bar{h} = \frac{1}{L} \cdot \sum_{i=1}^{L} h_i \tag{12}$$

for the two-dimensional simulations, and by

$$\bar{h} = \frac{1}{L^2} \cdot \sum_{i=1}^{L} \sum_{j=1}^{L} h_{ij} \tag{13}$$

for the three-dimensional simulations, where $L(L^2)$ is the total number of sites available for deposition on the target. Another quantity of interest is the average porosity ϵ, defined by

$$\epsilon = 1 - \frac{M}{\bar{h}} \tag{14}$$

where $M(=N/L,\ N/L^2$ for two- and three-dimensions, respectively) is the total number of particles deposited per surface site on average.

A width parameter for the active zone (Family and Vicsek, 1985), or (equivalently) a measure of the surface roughness, can be calculated from

$$\xi = \overline{\{(h_i - \bar{h})^2\}}^{1/2} = \left\{\frac{1}{L} \cdot \sum_{i=1}^{L} (h_i - \bar{h})^2\right\}^{1/2} \tag{15}$$

for two-dimensions and, similarly, for three dimensions

$$\xi = \left\{\frac{1}{L^2} \cdot \sum_{i=1}^{L} \sum_{j=1}^{L} (h_{ij} - \bar{h})^2\right\}^{1/2} \tag{16}$$

In the course of the two-dimensional simulations, we also calculate distributions of the pore size and pore area, where each pore is taken to consist of a connected cluster of unoccupied sites. The area of each pore is described by the number of voids in the pore, and its linear size is here simply defined as the square root of its total area. To identify the pores, we use an adaptation of the Hoshen-Kopelman algorithm (This algorithm allows the identification of connected clusters in a percolating lattice, requiring the storage at any time of only one row of the

lattice. Its use renders larger problems tractable.) (Hoshen and Kopelman, 1976). It is noteworthy that we compute and report the pore size distribution only for the main body of the deposit, because only this part has a closed (porous) structure. (The active zone has a very open, tree-like structure (Meakin et al., 1986) and, hence, the usual concept of porosity does not apply.)

In three dimensions, most of the pores are interconnected and so a different definition of a "pore" is necessary that takes into account both the pore itself and the pore mouths. Thus, in order to obtain a pore size distribution for the three-dimensional deposits we use the concept of the "void particles" (Debbas and Rumpf, 1966; Dullien, 1979). According to this model, the interconnected network of the void space is replaced with "void particles," obtained by severing the continuity of the channels at the "windows" (pore mouths) separating adjacent voids. By virtue of these concepts, we obtain a model of the pore space as an ensemble of individual void "particles" (Dullien, 1979).

The implementation of the model on the computer is quite straightforward. In the results we present, we assume the above-mentioned window size to be equal to one particle cross-section. In other words, we close connections between pores that are joined by channels of cross-section equal to one particle size. Initially, we examine every cross-section of the deposit (so for a deposit of macroscopic dimensions L × L × H, we will examine an equal number of cross-sections), and wherever we find such a window, e.g., a void whose four neighbors on the given plane (cross-section) are occupied, we fill it. In this way, we obtain the equivalent of Rumpf's collection of void particles, on which we apply the Hoshen-Kopelman algorithm to obtain the pore size distribution.

Results and Discussion

Two-dimensional simulations

To demonstrate the effect of the above-mentioned Peclet number on the resulting deposit microstructure, we present in Figure 2 three typical deposits. Each was grown on a 100-column 2D-square lattice, and each deposit contains 3,000 particles. In each case, the particles were generated ten rows over the top of the deposit, that is $H = 10$. The first deposit (Figure 2a) was formed by particles following straight line (pure ballistic) trajectories, so that $Pe = \infty$. It is found that the resulting structure is on the average uniform at all length scales; the active zone alone has the scaling properties associated with a *fractal* (Mandelbrot, 1983). An extended analysis of the properties of isotropic ballistic deposits may be found in Meakin et al. (1986). Figures 2b and 2c show deposits containing the same number of particles, but with Peclet numbers equal to 5.49 and 1.91, respectively (corresponding to $\kappa = 0.30$ and 0.60). Note that as the Peclet number decreases, i.e., as the importance of Brownian diffusion increases: (a) the structure becomes more open; (b) the average height of the deposit increases; and (c) tree-like patterns begin to appear. As the Peclet number continues to decrease, we approach the DLA model, and for $Pe = 0$, one obtains the characteristic DLA tree-like structures (Witten and Sander, 1981; Meakin, 1983).

We characterize the evolution of the deposit with time using the dependence of the average height $\bar{h}$ on the number of particles deposited for different values of the Peclet number. In the present simulations, it is justifiable to use time and number of deposited particles interchangeably, because deposition occurs

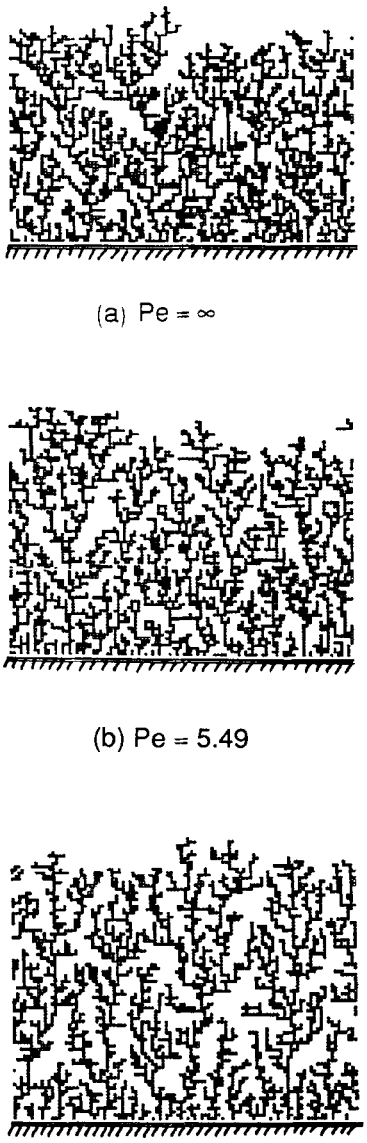

Figure 2. Typical two-dimensional deposits of about 3,000 particles on a 100 column-wide lattice.

Deposit (a) corresponds to $Pe = \infty$ (porosity, $\epsilon = 0.50$ and mean height, $h = 59.95$), deposit (b) to $Pe = 5.49$ ($\epsilon = 0.54$, $h = 64.91$), and deposit (c) to $Pe = 1.91$ ($\epsilon = 0.59$, $h = 73.75$).

at a constant rate. [If, on the other hand, the phoretic velocity (or equivalently the Peclet number) does not remain constant throughout the deposition process, then clearly physical time and number of deposited particles cease being proportional to each other. This would be the case if, for example, we allowed thermophoretic velocity to depend on the deposit surface temperature (Rosner and Nagarajan, 1987). Then, as the deposit grows, and depending on the relative importance of cooling/heating due to radiation, convection, and conduction, the surface temperature may decrease/increase, which would clearly change the Peclet number. In consequence, the deposit microstructure would also change. Note also that under such (commonly encountered) conditions, it may not be correct to infer deposition rates solely from deposit thermal resistance measure-

ments, e.g., deposition detectors (see, Marner and Henslee, 1984; Sum et al., 1987), since, as the deposition process continues, both the rate of deposition and the effective thermal conductivity of the deposit inevitably change.] In our simulations, $\bar{h}$ depended on N, the number of particles deposited, through a power law, that is

$$\bar{h} \sim N^{\nu} \tag{17}$$

where $\nu = 1.0$ for $Pe = \infty$ (pure ballistic case), and $\nu > 0$ for $Pe < \infty$. The value of $\nu = 1.00 \pm 0.02$ for the ballistic case is in agreement with the value found by Meakin et al. (1986) and corresponds to porous structure with no dependence of the porosity on any length scale, while $\nu > 1.0$ in the presence of diffusion suggests a fractal structure. In practice, this implies that, at least for the initial stage of deposition (before any collapsing or tearing of the tree-like structures begins to occur), the average height of the deposit exposed to the host fluid increases with the number of depositing particles in a nonlinear manner.

The active zone width, ξ, depends on the number of particles deposited per lattice site, M, in a different manner. For M small, or more quantitatively for

$$\frac{M}{L^{\gamma}} \ll 1 \tag{18}$$

where γ is a positive constant, the active zone width also exhibits a power law dependence, but as N becomes larger, it saturates at a constant value, which is a function of the target width, L, only. For an extensive analysis of the scaling properties of the active zone width see the paper by Family and Vicsek (1985).

In Figure 3, we plot mean height ($\bar{h}$) and surface roughness (ξ) vs. Peclet number for 2D deposits using log-log coordinates. The data shown are averaged from ten runs. All runs were for 50,000 particles grown on a lattice that is 400-columns-wide, with starting distance $H = 10$, and particle mean free path equal to unity. If we examine the dependence of mean height on Peclet number (upper curve in Figure 3), we can identify three regions: for $Pe > 10$, there is practically no dependence of mean height on the Peclet number. We find a power-law dependence with a small negative exponent which, due to the statistical error, can be assumed equal to zero.

$$\bar{h} \sim Pe^{-0.007 \pm 0.02} \tag{19}$$

The error limits given in Eq. 19 and in the rest of this communication were obtained from the variance of the slopes of the least square fits of 10 to 20 data samples. For $2 < Pe < 10$, there seems to be a transition zone, and again for $Pe < 2$, we obtain a stronger power-law dependence, that is

$$\bar{h} \sim Pe^{-0.267 \pm 0.04} \tag{20}$$

The active zone width or surface roughness exhibits a similar dependence on the Peclet number. For Peclet larger than about 10, there is again no significant dependence, for $2.0 < Pe < 10$, there is a transition regime, and for $Pe < 2.0$ we find

$$\xi \sim Pe^{-0.523 \pm 0.05} \tag{21}$$

We have also determined the pore *area* (PAD) and pore *size* distribution (PSD) of two-dimensional deposits generated under different deposition conditions. The first interesting feature of the PAD and the PSD is that for a given Pe value, if suitably normalized, both are independent of the actual deposit 'size', e.g., independent of the number of particles deposited, N, and, therefore, independent of *time*. To demonstrate this, we plot in Figure 4 normalized pore number vs. pore area, for various size ballistic deposits, grown on a lattice 400 columns wide. The normalization was achieved by dividing the number of pores of a

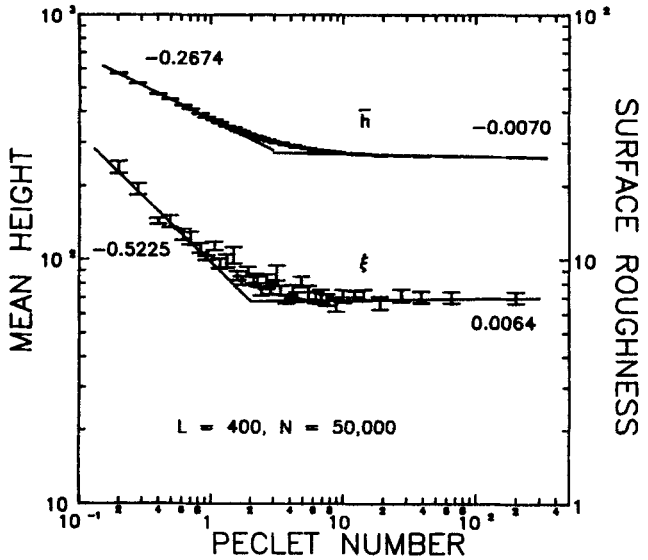

Figure 3. Dependence of average porosity and active zone width (surface roughness) on Peclet number.

All data correspond to 50,000 particle deposits grown on a 400 column-wide lattice.

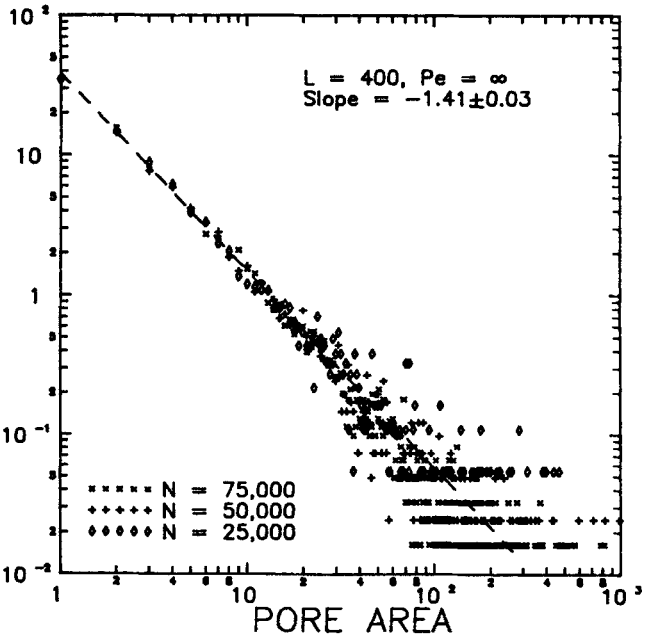

Figure 4. Invariance of pore area distribution with size of deposit at given Peclet number for two-dimensional deposits.

given area by the total number of pores. The slope of the straight line that fits the data was calculated, using only the pores of corresponding densities greater than 1%. The scatter that occurs for large pore sizes is due to the finite size of the deposit: i.e., we have simply too few large pores in our simulations to obtain significant statistics for them. We further find that there seems to be no dependence on the lattice width L of the resulting pore area distribution.

In Figure 5 we present a plot of number of pores of given size vs. pore size on log-log coordinates for $Pe = 8.89$ and 0.40, and for 100,000-particle deposits, grown on a 400-column-wide square lattice. As expected from the abovementioned N-invariance properties of the PSD, we find that the pore size density scales with a power of the pore size.

We can express the dependence of the pore number on pore size for any deposit by the local law

$$N_L(\text{pore size}) \sim (\text{pore size})^k \tag{22}$$

where we find that k varies from $k = -2.72 \pm 0.05$ for $Pe = \infty$ to $k = -3.54 \pm 0.06$ for $Pe = 0.40$. For deposits grown with Peclet less than 0.4 ($\kappa > 0.90$), the resulting structures are very open, the total number of pores is small, and hence larger simulations are necessary to obtain statistically significant results.

If we denote by $N_A(A)$ the pore area distribution function, then Eq. 22 can be rewritten as

$$N_A(A) = N_1 A^{-\alpha} \tag{23}$$

where N_1 is the number of pores of area equal to unity. Note that due to the definition of the characteristic length of a pore (to be equal to the square root of its area), we have

$$k = 2\alpha \tag{24}$$

As is demonstrated by Figure 4, the percentage of pores of unit area is independent of the number of particles deposited.

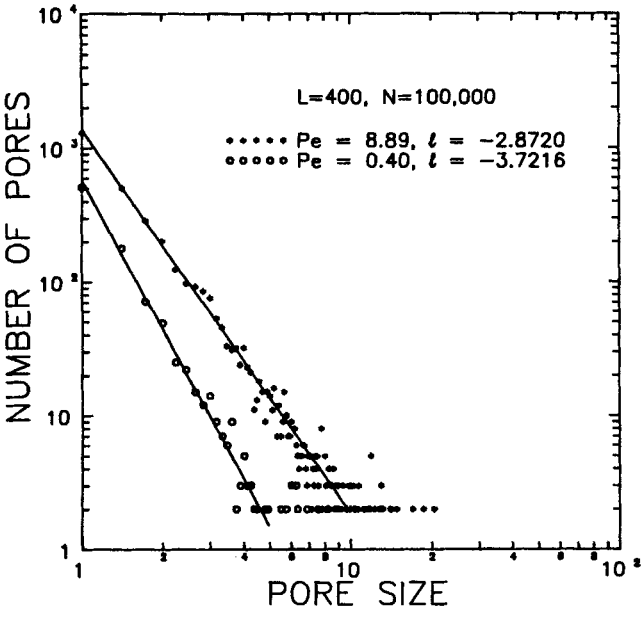

Figure 5. Number of pores *vs.* pore size (pore size distribution function) for $Pe = 8.89$ and $Pe = 0.40$.

We can exploit this observation to determine how well the pore area distribution obeys the proposed scaling relationship, e.g., Eq. 23. If we denote by C the percent of pores of unit size, then clearly:

$$C = \frac{N_1}{N_{\text{tot}}} = \frac{N_1}{\int_1^{A_{\max}} N_1 A^{-\alpha} dA} = \frac{1-\alpha}{A_{\max}^{1-\alpha} - 1} \tag{25}$$

where $A_{\max}$ is the area of the largest pore expected to be present in the given deposit. Equation 25 should be satisfied for any deposit independent of its size. Hence, in the limit of a very large deposit, we have

$$A_{\max} \gg 1 \tag{26}$$

or, since α is greater than unity,

$$A_{\max}^{1-\alpha} - 1 \approx -1 \tag{27}$$

Substituting Eq. 27 into Eq. 25, we obtain

$$\alpha - C = 1 \tag{28}$$

To check whether Eq. 28 is satisfied, we give in Table 1 the measured slope of the PAD, e.g., α, the percent of pores of unit area and their difference. Note that, in every case and within the statistical error, Eq. 28 is satisfied.

The exponent α can be also related to the density, ρ, of a deposit. The deposit density is given by (see also Eq. 14)

$$\rho = \frac{N}{A_{\text{tot}} + N} \tag{29}$$

where $N \equiv$ total number of particles in the deposit, A_{tot} the total pore (void) area. From Eq. 24, if we integrate over all the pores in the deposit we find that

$$A_{\text{tot}} = \int_1^{A_{\max}} N_A(A) A dA = \frac{N_1}{2-\alpha}(A_{\max}^{2-\alpha} - 1) \tag{30}$$

with $A_{\max}$ an upper cutoff, representing the area of the largest pore, expected to be present in a given deposit. ($A_{\max}$ can be also regarded as a free parameter that can be 'tuned' to best fit actual deposit properties.) We find that $A_{\max}$ is a weak function of the deposit size. Combining now Eqs. 29 and 30, we get

$$\frac{1-\rho}{\rho} = \frac{A_{\text{tot}}}{N} = \frac{N_1}{N}\frac{1}{2-\alpha}(A_{\max}^{2-\alpha} - 1) \tag{31}$$

Table 1. Verification of Power-Law Scaling of the Pore Area Distribution

Pe	$C = N_1/N_{\text{tot}}$	α	$\alpha - C$
∞	0.348	1.36 ± 0.05	1.01 ± 0.05
8.89	0.362	1.40 ± 0.05	1.04 ± 0.05
0.40	0.618	1.77 ± 0.05	1.09 ± 0.06

Note that from Eq. 27 it is possible to obtain the exponent α, and hence the complete pore area/size distribution, given the deposit density, and the total number of pores of area equal to unity, without having to analyze the whole deposit, using the Hoshen-Kopelman algorithm. Finally the power law form of the PSD suggests that it may be possible to develop a mean field theory to estimate the transport properties of deposits grown at different Peclet numbers.

The stochastic simulation approach we employ can be further generalized to account for polydisperse particle *populations* and nonspherical particle *orientation*. It has recently been shown that under typical optical wave guide preform deposition conditions, which include thermophoretically dominated submicron particle deposition at high particle mass loadings, Brownian coagulation is the dominant factor in determining the size distribution of the depositing particles (Park and Rosner, 1989) even though thermophoresis dominates Brownian diffusion in determining total mass deposition rates (Rosner and Park, 1988). In Figure 6, we show two deposits grown due to a purely thermophoretic mechanism, e.g., the Peclet number goes to infinity. These deposits are generated by particle populations with size distributions similar to the one predicted by Park and Rosner (they calculate a discrete size distribution that contains up to 'hexamers'). In the first deposit, we assume that all particles come down with their long axis vertical, while in the second deposit 50% come down with their long axis vertical and the rest with their long axis horizontal. Compare also with the deposit in Figure 2a, which is generated from a monodisperse (single-size) particle population. We should also point out that all three deposits contain the same number of *primary* particles. Note that the structures of Figures 2a and 6 are different from each other (Note also the difference in average height and corresponding porosity of each deposit. For example, the porosity of the deposit of Figure 6b is much closer to the porosity of the deposit of Figure 2c, even though the latter was generated with $Pe = 1.67$). It is also likely that their transport properties will be different as well. For example, it should be possible to compare the effective thermal conductivity of deposits such as those of Figures 6a and 6b in order to establish quantitative laws of the effect of polydispersity and particle orientation distribution on the properties of the resulting particulate deposits.

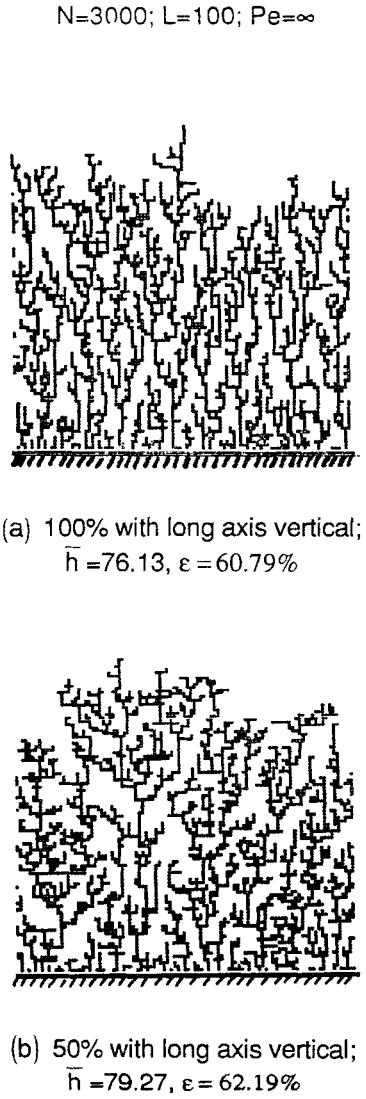

Figure 6. Effect of polydispersity of generating particle population and orientation of the incoming particles on the structure of the resulting deposit.

Three-dimensional simulations

We have 'grown' three-dimensional deposits, under various deposition conditions. It is interesting to note that in most cases the qualitative behavior in two and three dimensions is the same. Thus, again, the average height scales with the number of particles deposited in a power law manner (see also Eq. 17), where the actual exponent depends on the local Peclet number and, as before, is equal to unity only in the pure ballistic case ($Pe \rightarrow \infty$); that is, only under such deposition conditions is the resulting structure macroscopically porous (nonfractal). In Figure 7 we plot mean height vs. number of particles for three-dimensional deposits grown on a 30 × 30 orthogonal lattice, with different

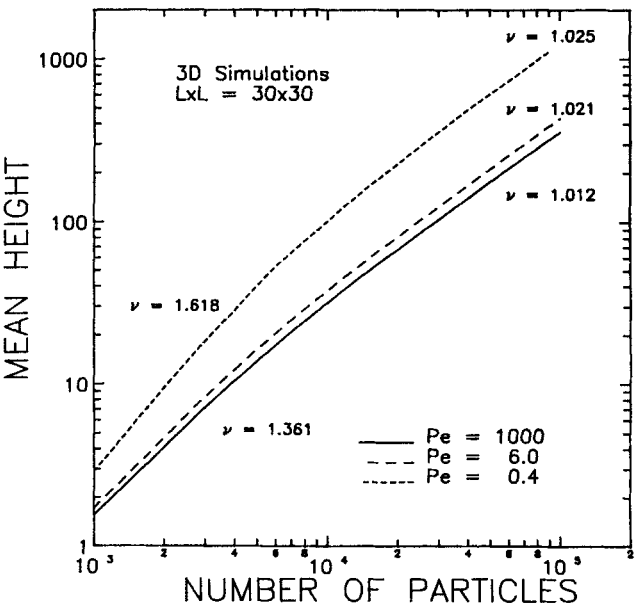

Figure 7. Deposit mean height *vs.* number of particles deposited for three-dimensional deposits, generated at different Peclet numbers.

Peclet numbers. The data are averaged from 20 runs. Note the strong dependence of the exponent ν on Pe during the initial stages of deposition. On the other hand, as the deposit height becomes much larger than the lattice size, L, the deposit structure (properties) approaches a steady state, as indicated by values of ν close to unity independent of Pe. The active zone width of three-dimensional deposits exhibits also the same dependence on number of particles deposited as in two dimensions, as discussed earlier.

A difference between two- and three-dimensional deposits exists in the higher degree of openness of the latter. In Figure 8 we show a vertical and a horizontal cross-section of a three-dimensional deposit, grown on a 30 × 30 orthogonal lattice and containing 25,000 particles. This deposit was formed with Pe = 4.0 (corresponding to $\kappa = 0.50$). Cross-sections of an equal-size deposit, grown under purely ballistic conditions, is shown in Figure 9a. Note the openness of these structures. (Compare also with the two-dimensional deposits of Figure 2.)

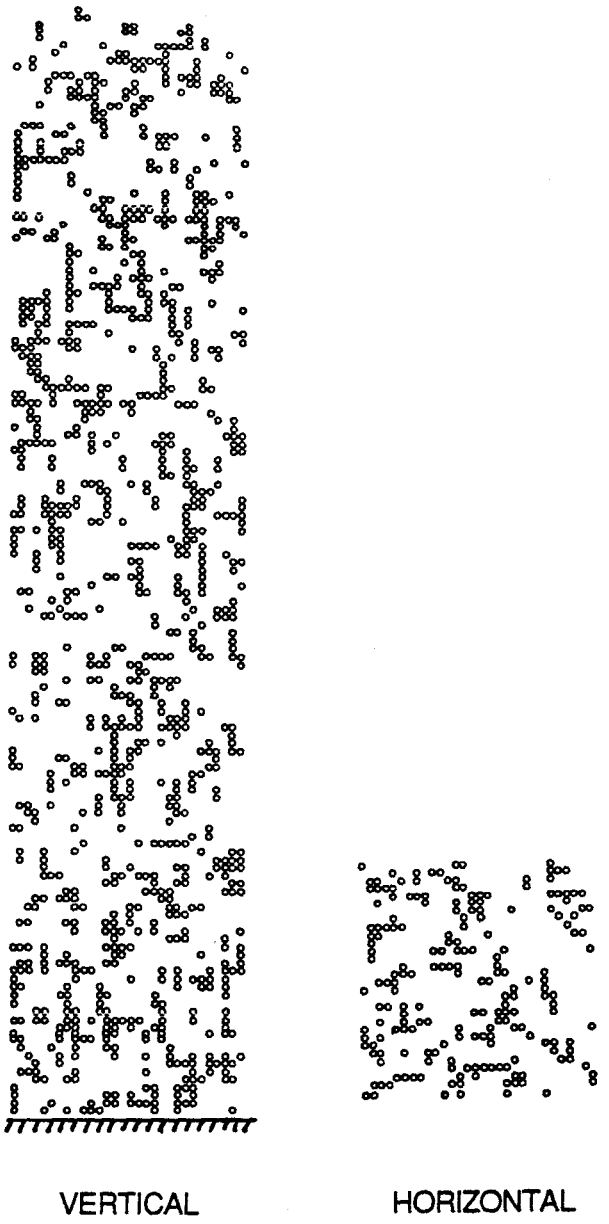

Figure 8. Typical horizontal and vertical cross-sections of a three-dimensional deposit of about 25,000 particles grown on a 30 × 30 cubic lattice with Pe = 4.0.

In Figure 10 we plot deposit mean height and surface roughness vs. Peclet number for three-dimensional deposits, grown on 30 × 30 orthogonal lattices and each containing 70,000 particles. As before, for Peclet number greater than 10, both porosity and surface roughness remain about constant; e.g., the deposits obtained under such conditions are ballistic-like independent of the actual Peclet number, and it is only for lower Peclet values that diffusion becomes dominant and more open tree-like structures evolve.

In the lower Peclet regime ($Pe < 2.0$), one can again employ power-law-type expressions to describe the dependence of deposit mean height and surface roughness on Peclet number. We find that

$$\bar{h} \sim Pe^{-0.475 \pm 0.05} \tag{32}$$

and

$$\xi \sim Pe^{-0.756 \pm 0.04} \tag{33}$$

To obtain pore size distributions of three dimensional deposits we employ the concept of the void particles, as described previously. In Figure 9 we show the same vertical and horizontal cross-sections of a three-dimensional 40,000 particles deposit

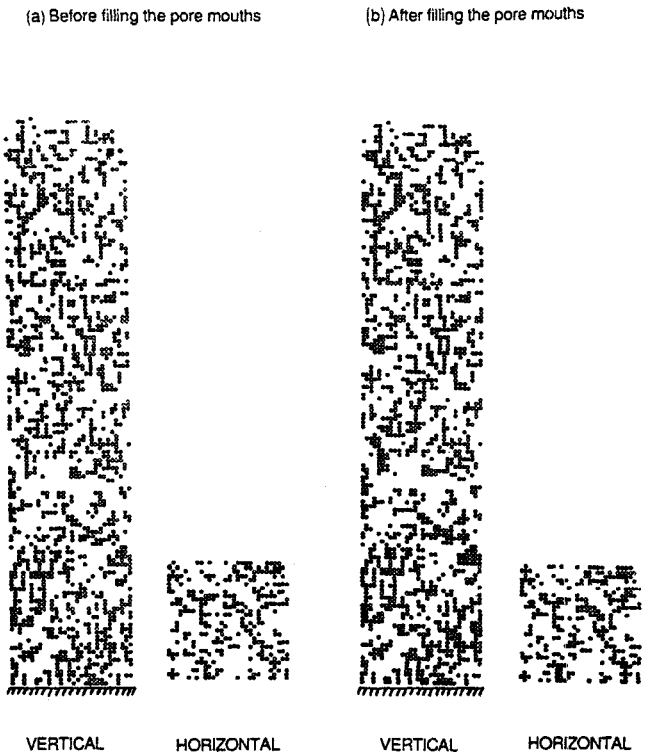

Figure 9. Horizontal and vertical cross-sections of a three-dimensional deposit ($L \times L = 30 \times 30$, $N = 40{,}000$).

They were generated under pure ballistic conditions: (a) before filling the pore mouths and (b) after filling. The porosity before was 0.68 and after 0.67.

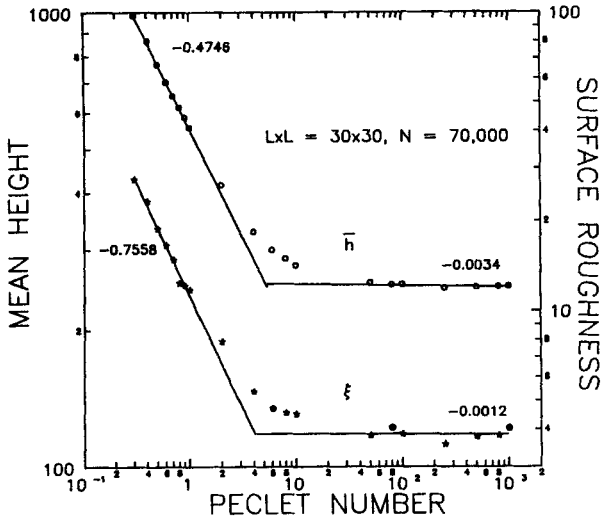

Figure 10. Dependence of average porosity and active zone width (surface roughness) on Peclet number.

All data correspond to 70,000 particle deposits grown on a 30 × 30 lattice.

generated under pure ballistic conditions on a 30 × 30 orthogonal lattice, before filling the pore mouths (Figure 9a) and after filling them (Figure 9b). Note that the original and the transformed deposit, "look" practically identical. In a more quantitative way, we find that the density increase of the transformed deposit due to the filling of the windows is always less than 2.5%. Based on these observations, we argue that the pore size distribution, which we calculate from the transformed deposit, represents the collection of voids present in the original deposit.

In Figure 11, we plot number of pores vs. pore volume for 250,000 particles deposits, grown on 30 × 30 orthogonal lattices

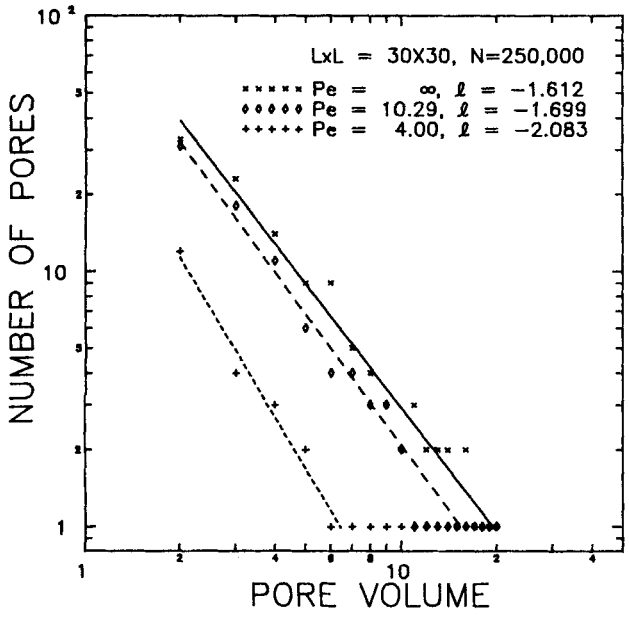

Figure 11. Pore volume distribution function of three dimensional deposits, grown at different Peclet numbers.

with different Peclet numbers. Again, the number of pores of given volume, or equivalently the number of pores of given characteristic size, where we define the characteristic size as the cube root of the volume, scale in a power law manner, namely

$$N_L(\text{pore size}) \sim (\text{pore size})^{-k} \tag{34}$$

where k is an increasing function of Pe.

Another important factor that affects the structure of the deposit is the mean-free path of the arriving particles. As already mentioned, the assumption of a particle jump distance (step), l, smaller or equal to the particle size holds only for Stokesian particles. For a so-called Knudsen ('highly dispersed') aerosol, the mean free path is much larger than the particle size,

$$l > a \tag{35}$$

and thus the local mean free path introduces a new length scale. For pure DLA deposits, it has been shown that the introduction of a particle jump distance larger than the actual particle size or equivalently lattice size results in structures that exhibit a crossover in their properties (see Bensimon et al., 1983; Jullien and Botet, 1987). Thus, deposits grown under such conditions, while compact at small length scales (with properties similar to the properties of "ballistic" deposits), at larger scales (when their macroscopic dimension becomes larger than the particle step size) approach the DLA limit.

From the above arguments, it is clear that in the general case of deposition of a Knudsen aerosol due to combination of Brownian diffusion and phoresis, there will be two opposing factors influencing the actual structure and hence, properties of the resulting deposit. While the random motion of the particles will enhance the appearance of ramified structures, at the same time, the large particle mean-free-path will have a stabilizing and compacting effect.

In Figure 12, we plot deposit mean height (lower curve) and surface roughness (upper curve) vs. Peclet number for three-dimensional deposits, generated by particles performing random walks with a dimensionless mean free path equal to three. The deposits were grown on 30 × 30 orthogonal lattices, and each contained 70,000 particles. Each data point was obtained by averaging over 20 realizations. The following observations can be made:

i) The introduction of this new length scale does not alter the structure of deposits corresponding to large Peclet values. So, for example, the mean height and surface roughness of deposits grown with Pe greater than about ten are independent of the mean free path. (Compare also with Figure 10, which shows the equivalent data for particle mean free path equal to unity.) This statement is of course identically true for deposits grown under pure ballistic conditions.

ii) For Peclet values around 10.0 and below, a second order transition occurs, and the corresponding deposits begin to grow faster and hence become more open.

iii) At Peclet values less than about 2, the deposit properties become again only weak functions of the Peclet number. For mean-free path equal to three and for $Pe \ll 1$, we find for the dependence of the deposit mean height on the Peclet number:

$$\bar{h} \sim Pe^{-0.038 \pm 0.02} \tag{36}$$

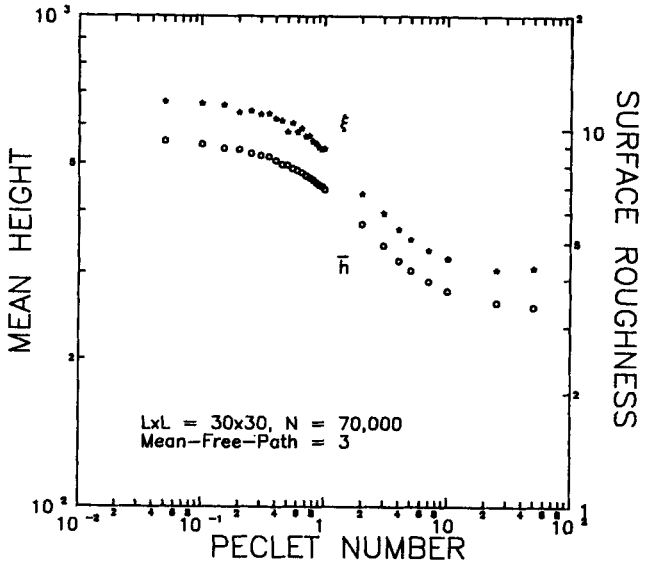

Figure 12. Deposit mean height, and surface roughness *vs.* Peclet number for three-dimensional deposits generated by particles following trajectories with mean free path equal to three particle diameters.

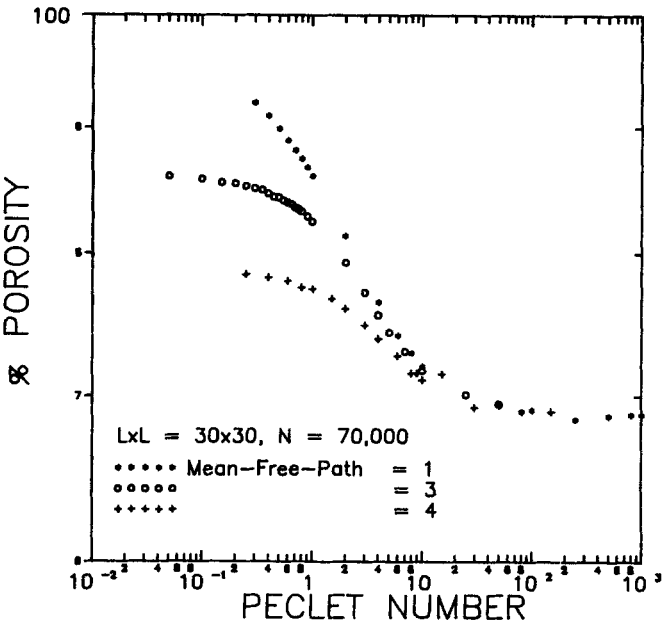

Figure 13. Deposit porosity *vs.* Peclet number for deposits generated by particles following trajectories with different particle-mean free paths.

and for the surface roughness,

$$\xi \sim Pe^{-0.044\pm0.01} \tag{37}$$

where again, the exponents we find, statistically speaking, are not distinguishable from zero. Compare also with Eqs. 20 and 21, which show the dependence of mean height and surface roughness on the Peclet number for the case of mean free path equal to unity.

In Figure 13, we plot final deposit porosity vs. Peclet number, for different values of the particle mean-free path. Like before, all deposits contained 70,000 particles and were generated on 30 x 30 cubic lattices. It is interesting to note that the critical Peclet value (where the transition occurs) seems to be independent of the mean-free-path. On the other hand, the saturation value of the porosity, approached for small *Pe*, is a sensitive function of the mean-free-path. The trend that our results exhibit for large mean-free-path values are in agreement with the results of Jullien and Botet (1987), which suggest that even in the case of pure diffusion-limited aggregation, if the particle mean-free path remains larger than some characteristic dimension of the growing deposit, then the deposit properties will always be ballistic-like.

To conclude, we would like to reexamine the results we have obtained using as a framework the *screening length model* (Hentschel, 1984; Houi and Lenormand, 1984). Note that we are not proposing a theory to predict quantitatively actual properties of the growing deposits. Rather, we feel that the screening length model, in spite of its simplicity, presents an intuitive way to rationalize the dependence of the growing deposits and their properties on the Peclet number and mean-free-path.

Consider a particle that is performing a random walk in the vicinity of an existing deposit. The screening length is defined as the distance the particle can penetrate into the growing aggregate before it gets captured. Suppose that a particle will take on average, N_w steps in the vicinity of the deposit before it gets captured. Then it is straightforward to show that the expected distance traveled toward the target (say y direction in Figure 1) in N_w steps is (Eq. 5):

$$E[y] = (1 - \kappa)N_w l \tag{38}$$

In this time interval (steps), the expected distance traveled in directions parallel to the target (direction x of Figure 1) is

$$E[x] = \left(\left(\frac{\kappa(2-\kappa)}{2d}\right) l^2 N_w\right)^{1/2} \tag{39}$$

In general, we now would expect to obtain a ballistic-like, i.e., compact deposit, if the incoming particles penetrated deeply into the active zone before they were captured, since in that case the active zone would essentially become filled as the deposit grew, causing the deposit density to remain bounded. Thus, one way of telling *a priori* whether a deposit will evolve towards a porous or a fractal structure is to examine the ratio of the expected distance traveled by an incoming particle in the transverse direction, $E[x]$, to the distance traveled into the deposit, $E[y]$.

If we solve Eq. 38 for N_w and substitute into Eq. 39, we obtain for $E[x]$:

$$E[x] = \left(\frac{\kappa(2-\kappa)}{2d(1-\kappa)} l E[y]\right)^{1/2} \tag{40}$$

or

$$\frac{E[x]}{E[y]} = \left(\frac{\kappa(2-\kappa)}{2d(1-\kappa)} \frac{l}{E[y]}\right)^{1/2} = \left(\frac{1}{Pe} \frac{l}{E[y]}\right)^{1/2} \tag{41}$$

Note that the righthand side of Eq. 41 is the square root of the inverse of the original Peclet number (before assuming both the characteristic length, δ_m, and the particle-mean-free path, l, equal the particle size) as defined by Eq. 7, where the characteristic length δ_m (which was introduced in order to satisfy dimensional constraints, but had no apparent physical meaning) becomes in this context the distance a particle penetrates into the deposit before it gets captured. If we denote Y to be the depth of the active zone, then the growing deposit will remain ballistic-like as long as

$$Y < E[y] \tag{42}$$

or, making use of Eq. 41, provided

$$\frac{E[x]}{E[y]} = \left(\frac{1}{Pe}\frac{l}{E[y]}\right)^{1/2} < \frac{E[x]}{Y} \tag{43}$$

From Eq. 41, it is clear that the deposit ceases to be porous below a critical Peclet number, where inequality (Eq. 41) no longer holds. This accounts for the insensitivity of the deposit properties to Peclet number, at Peclet numbers larger than a critical value. (See, e.g., Figures 10 and 13.)

Finally, in the case of mean-free-path larger than unity, the number of steps, N_w, a particle takes (number of times it changes its direction) before it gets captured, is on the average smaller than in the case of $l = 1$, and so the particle "samples" less space, as it moves into the deposit. This results in a finite penetration depth, which in the worst case will be of the order of one mean-free-path, and so, for $Pe \to 0$, the deposit density saturates at a small value, which is still greater than zero.

Conclusions and Implications

In this paper, we have outlined a rational theoretical model capable of describing deposit evolution processes under a variety of mechanistic conditions of practical importance. We have assumed that the arriving particle trajectory can be described by the superposition of a deterministic motion and a random motion, and have expressed their relative importance in terms of an appropriate Peclet number. Furthermore, we identified the parameters that may be important in determining the structure of the resulting deposits and have demonstrated their effect. Thus, we found that polydispersity of the depositing particles (see, e.g., Rosner, 1989) can significantly increase the openness of the resulting structure, while a large particle-mean-free path, e.g., larger than the actual particle size, results in more compact, less porous deposits. Even in its present elementary form (on-lattice simulations with sticking probability equal to unity), we believe this formulation is promising because it possesses enough realism and degrees of freedom to incorporate the competing mechanisms known to occur during technologically important particulate deposition processes. We have also determined (for the first time to our knowledge) pore size distributions for the resulting deposits in both two- and three-dimensions, and determined that they are independent of deposit size if normalized properly, and that they have a power-law form, with the actual exponent depending on Pe. In this connection, it is interesting to point out that the pore spaces of sandstone have been experimentally measured (Katz and Thompson, 1985; Krohn and Thompson, 1986), and they are indeed fractal. Such sandstone growth is presumed to depend on chemical kinetic parameters, but it may be possible to employ similar techniques to measure the pore size distribution of particulate deposits.

The present work is but a first step toward the ultimate ambitious goal of somehow establishing rational, general, quantitative relationships between particle (and vapor) deposition *mechanisms* and resulting *deposit microstructures*. Iterative comparisons with experimentally observed microstructural information and resulting deposit properties will have to be made in order to assess and improve essential features of this convenient modeling approach—e.g., the 'active-site' sticking submodel. Moreover, further work will clearly be required: a) to understand situations in which the deposition mechanisms evolve with time; b) to obtain the needed information on the transport properties (effective permeability, thermal conductivity, etc.) of the resulting deposits; and c) to understand deposits which gradually evolve due to, say, sintering. Fortunately, such information promises to be applicable to a wide variety of technologies of current and future importance, whether the deposits are undesired ('fouling') or desired.

Appendix A

The diffusion coefficient for a d-dimensional asymmetric random walk can be defined by (Eq. 6):

$$D_B = \frac{\overline{(x - \bar{x})^2}}{2dt} \tag{A1}$$

where the mean displacement, $\bar{x}$, is equal to

$$\bar{x} = p_1x_1 + p_2x_2 + \cdots + p_{2d}x_{2d} = (p_1u_1 + p_2u_2 + \cdots + p_{2d}u_{2d})l \tag{A2}$$

and, u_i, is the unit vector along the ith direction. It is straightforward to show that in general we can label the 2d possible directions of our coordinate system in such a way, so that

$$u_i = -u_{i+d} \tag{A3}$$

Combining now Eqs. A2 and A3, we obtain for the mean displacement:

$$\bar{x} = (1 - \kappa)l \tag{A4}$$

Note also that

$$\overline{x^2} = (p_1u_1^2 + p_2u_2^2 + \cdots + p_{2d}u_{2d}^2)l^2 = \left(\frac{\kappa}{2d}(u_1^2 + u_2^2 \cdots + u_{2d}^2) + (1 - \kappa)u_1^2\right)l^2 = l^2 \tag{A5}$$

So, for the Brownian coefficient, calculated after n steps, we obtain:

$$D_B = \frac{\overline{x^2} - (\bar{x})^2}{2dt} = \frac{(l^2 - (1 - \kappa)^2l^2)n}{2dn\tau} \tag{A6}$$

or equivalently

$$D_B = \frac{\kappa(2 - \kappa)l^2}{2d\tau} \tag{A7}$$

Acknowledgments

This research was supported, in part, by the U.S. Department of Energy-Pittsburgh Energy Technology Center via Grant DE-FG22-86 PC 90756 and the 1988 Industrial Affiliates of the Yale High Temperature Chemical Reaction Engineering (HTCRE) Laboratory (Shell Foundation, SCM-Chemicals, Lycoming-Textron). Acknowledgment is also made to the Donors of the Petroleum Research Fund, administered by the American Chemical Society, for partial support (J. O'Brien) of this research. The authors would also like to thank Drs. P. Garcia Ybarra, J. Castillo, T. Vicsek, and J. Fernandez de la Mora for their comments and helpful discussions throughout this work.

Notation

a = particle size
A = pore area (in two-dimensions)
A_{max} = area of largest pore
c = particle drift velocity
C = fraction of pores of unit size
d = dimensionality of the lattice
D_B = Brownian diffusion coefficient
$E[x]$ = expected distance traveled in x-direction
h = height
$\bar{h}$ = mean height
H = starting distance
k = exponent that characterizes dependence of pore size distribution function on pore size
l = particle mean-free-path
L = linear dimension of lattice
M = number of particles per column
n = number of steps
N = total number of particles
N_1 = number of pores of unity area (two dimensions)
N_A = pore area distribution function
N_L = pore size distribution function
N_{tot} = total number of pores
N_w = number of steps
p = probability
Pe = Peclet number
Re = Reynolds number
Sc = particle Schmidt number
t = time
u = unit vector
V = deterministic velocity
x, y = directions
x = particle position vector
$\bar{x}$ = mean displacement
Y = depth of the active zone

Greek letters

α = exponent that characterizes dependence of pore area distribution function on pore area
δ_m = characteristic length scale
ϵ = porosity
γ = positive constant
κ = probability of diffusing
ν = exponent that characterizes dependence of mean height on number of particles
ρ = deposit density
τ = time step
ξ = surface roughness

Subscripts

i = ith direction or ith column
ij = ijth column

Abbreviations

DLA = diffusion-limited aggregation
NN = nearest neighbor
PAD = pore area distribution
PSD = pore size distribution

Literature Cited

Albers, J., J. M. Deutch, and I. Oppenheim, "Generalized Langevin Equations," *J. Chem. Phys.*, **54**(8), 3541 (1970).

Baumgartner, H., and F. Löffler, "Three-Dimensional Numerical Simulation of the Deposition of Polydisperse Aerosol Particles on Filter Fibers—Extended Concept and Preliminary Results," *J. Aerosol Sci.*, **18**(6), 885 (1987).

Bensimon, D., E. Domany, and A. Ahavony, "Crossover of Fractal Dimension in Diffusion-Limited Aggregates," *Phys. Rev. Lett.* **51**(15), 1394 (1983).

Castillo, J. L., D. Mackowski, and D. E. Rosner, "Photophoretic Contribution to the Transport of Absorbing Particles across Combustion Gas Boundary Layers," ACS Mg., *Symp. on Ash Deposition*, Dallas (Apr. 9–14, 1989).

Davies, C. N., ed., *Aerosol Science*, Academic Press, New York (1966).

Debbas, S., and H. Rumpf, "On the Randomness of Beds Packed with Spheres of Irregular Shaped Particles," *Chem. Eng. Sci.*, **21**, 583 (1960).

Dullien, F. A. L., *Porous Media*, Academic Press, New York (1979).

Family, F., and D. P. Landau, eds., *Kinetics of Aggregation and Gelation*, Elsevier (1984).

Family, F., and T. Vicsek, "Scaling of the Active Zone in the Eden Process on Percolation Networks and the Ballistic Deposition Model," *J. Phys. A: Math Gen.*, **18**, 275 (1985).

Fernandez de la Mora, J., and D. E. Rosner, "Inertial Deposition of Particles Revisited and Extended: Eulerian Approach to a Traditionally Lagrangian Problem," *J. PhysicoChem. Hydrody.*, **2**, 1 (1981).

Friedlander, S. K., *Smoke, Dust and Haze-Fundamentals of Aerosol Behavior*, Wiley, New York (1977).

Fuchs, N. A., *The Mechanics of Aerosols*, MacMillan (1964).

Garcia-Ybarra, P., and D. E. Rosner, "Thermophoretic Properties of Nonspherical Particle and Large Molecules," *AIChE J.*, **35**(1), 139 (1989).

Gökoglu, S. A., and D. E. Rosner, "Prediction and Rational Correlation of Thermophoretically Reduced Particle Mass Transfer to Hot Surfaces across Laminar or Turbulent Forced-Convection Gas Boundary Layers," *ChE Commun.*, **44**, 107 (1986).

Gökoglu, S. A., and D. E. Rosner, "Thermophoretically Augmented Mass Transfer to Solid Walls across Laminar Boundary Layers," *AIAA J.*, **24**(1), 172 (1986).

Goren, S. L., "Thermophoresis of Aerosol Particles in the Laminar Boundary Layer on a Flat Plate," *J. Coll. & Interf. Sci.*, **61**(1), 77 (1977).

Gupta, D., and M. H. Peters, "A Brownian Dynamic Simulation of Particle Deposition onto Spherical Collectors," *J. of Coll. & Interf. Sci.*, **104**(2), 375 (1984).

Hentschel, H. G. E., "Fractal Dimension of Generalized Diffusion-Limited Aggregates," *Phys. Rev. Lett.*, **52**(3), 212 (1984).

Hoshen, J., and R. Kopelman, "Percolation and Cluster Distribution I: Cluster Multiple Labeling Technique and Critical Concentration Algorithm," *Phys. Rev. B*, **14**, 3430 (1976).

Houi, D., and R. Lenormand, *Kinetics of Aggregation and Gelation*, F. Family and D. P. Landau, eds., Elsevier, 173 (1984).

Jullien, R., and R. Botet, *Aggregation and Fractal Aggregates*, World Scientific, 66 (1987).

Kapral, R., S. G. Whittington, and R. C. Desai, "Aggregation at a Surface: Crossover Behavior in a Biased Diffusion Model," *J. Phys. A: Math Gen.*, **19**, 1727 (1986).

Katz, A. J., and A. H. Thompson, "Fractal Sandstone Pores: Implications for Conductivity and Pore Formation," *Phys. Rev. Lett.*, **54**(12), 1325 (1985).

Krohn, C. E., and A. H. Thompson, "Fractal Sandstone Pores: Automated Measurements Using Scanning Electron-Images," *Phys. Rev.*, **B33**, 6366 (1986).

Mandelbrot, B. B., *The Fractal Geometry of Nature*, Freeman, San Francisco (1983).

Marner, W. J., and S. P. Henslee, "A Survey of Gas-Side Fouling Measuring Devices," Jet Propulsion Laboratory, Pasadena, CA, *JPL Publication* 84-11, DOE/ID-12138-3 (Mar., 1984); see, also, W. J. Marner and K. S. MacDavid, "Development of the Gas-Side Fouling Measuring Device," Jet Propulsion Laboratory Pasadena, CA, *JPL. Report* D-4065 (May, 1987).

Meakin, P., P. Ramanlal, L. M. Sander, and R. C. Ball, "Ballistic Deposition on Surfaces," *Phys. Rev.* **A34**(6), 5091 (1986).
Meakin, P., "Diffusion Controlled Deposition on Fibers and Surfaces," *Phys. Rev.*, **A27**(5), 2616 (1983).
Park, H. M., and D. E. Rosner, "Effects of Coagulation in the Boundary Layer on the Size Distribution of Thermophoretically Deposited Particles," *Chem. Eng. Sci.* (in press, 1989).
Park, H. M., and D. E. Rosner, "Combined Inertial and Thermophoretic Effects on Particle Deposition Rates in Highly Loaded Dusty Gas Systems," *Chem. Eng. Sci.*, in press (1989).
Peters, M. H., R. U. Jalan, and D. Gupta, "A Dynamic Simulation of Particle Deposition on Spherical Collectors," *Chem. Eng. Sci.*, **40,** 723 (1985).
Rosner, D. E., *Transport Processes in Chemically Reacting Flow Systems,* Butterworth, Stoneham, MA (1986, 1988).
Rosner, D. E., "Total Mass Deposition Rates from 'Polydispersed' Aerosols," *AIChE J.*, **35**(1), 164 (1989).
Rosner, D. E., and S. S. Kim, "Optical Experiments on Thermophoretically Augmented Submicron Particle Deposition from 'Dusty' High Temperature Gas Flow," *Chem. Eng. J.*, **29**(3), 145 (1984).
Rosner, D. E., and R. Nagarajan, "Towards a Mechanistic Theory of Net Deposit Growth from Ash-Laden Flowing Combustion Gases: Self-Regulated Sticking of Impacting Particles and Deposit Erosion in the Presence of Vapor 'Glue'," *Proc. Nat. Heat Trans. Conf., AIChE Symp. Ser.*, R. W. Lyczkowski, ed., **83**(257), 289 (1987).
Rosner, D. E., and H. M. Park, "Thermophoretically Augmented Mass, Momentum, and Energy Transfer Rates in High Particle Mass-Loaded Laminar Forced Convection Systems," *Chem. Eng. Sci.*, **43,** 2689 (1988).
Stanley, H. E., and N. Ostrowsky, *On Growth and Form,* M. Nijhoff Pub. (1986).
Sun, Y. I., S. R. Kale, R. A. Bajura, T. W. Keech, Jr., "Development of Thermopile Based Deposition Sensor" *ASME-HTD* **71,** 2414, Nat. Heat Transf. Conf. (1987).
Tien, C., "Aerosol Filtration in Granular Media," *Chem. Eng. Comm.*, **17,** 361 (1982).
Tien, C., C. S. Wang, and D. T. Barot, "Chainlike Formation of Particle Deposits in Fluid-Particle Separation," *Sci.*, **193,** 983 (1977).
Vold, M. J., "Computer Simulation of Floc Formation in a Colloidal Suspension," *J. Coll. Sci.*, **18,** 684 (1963).
Witten, T. A., and L. M. Sander, "Diffusion Limited Aggregation, a Kinetic Critical Phenomenon," *Phys. Rev. Letters,* **47**(19), 1400 (1981).

Manuscript received June 2, 1988, and final revision received Feb. 28, 1989.